Hybridization of Polymeric Micelles in a Dispersion Mixture

Ping Cai,[†] Chengqing Wang,[§] Jing Ye,[‡] Zuowei Xie,*[,†,‡] and Chi Wu*[,†,‡,§]

Shanghai-Hong Kong Joint Laboratory in Chemical Synthesis, Shanghai Institute of Organic Chemistry, Chinese Academy of Sciences, 354 Fenglin Lu, Shanghai 200032, China; Department of Chemistry, The Chinese University of Hong Kong, Shatin, N.T., Hong Kong; and The Open Laboratory of Bond Selective Chemistry, Department of Chemical Physics, University of Science and Technology of China, Hefei, Anhui, China

Received September 3, 2003; Revised Manuscript Received February 24, 2004

ABSTRACT: In a selective solvent, *n*-hexane, diblock coil−rod-like copolymers poly(ferrocenyldimethylsilane-*block*-dimethylsiloxane) (PFS-*b*-PDMS) can form spherical core−shell polymer micelles with an insoluble and aggregated PFS core and a soluble swollen PDMS shell. The micelles become larger with an increasing PFS content. The mixture of two dispersions made of PFS_{138}-*b*-$PDMS_{702}$ and PFS_{235}-*b*-$PDMS_{837}$ results in hybridization of these two kinds of block copolymer chains. The hybridization kinetics was studied by a combination of static and dynamic laser light scattering. As soon as the two micelle dispersions were mixed, larger hybrid micelles made of PFS_{138}-*b*-$PDMS_{702}$ and PFS_{235}-*b*-$PDMS_{837}$ were formed at the expense of each kind of the "pure" micelles. The hybridization can be attributed to the entropy gain as well as the space filling because the PFS block is rigid and rodlike.

Introduction

Polymeric core−shell micelles can be formed through the self-assembly of diblock or triblock copolymers in a solvent selectively good for only one block.[1−4] Most of the past experimental and theoretical studies of polymeric micelles dealt with their thermodynamic equilibrium structures.[5−11] The formation kinetics of polymeric micelles is less understood. For a given pair of block copolymer and selective solvent, there exists a critical micelle concentration (cmc). The number of copolymer chains inside each micelle at thermodynamic equilibrium is determined by a delicate balance between the changes of the enthalpy and entropy.[12] The change of the Gibbs free energy of inserting one copolymer chain into the micelle determines whether a polymeric micelle can be formed. It is the decrease of entropy that leads to the cmc. In a stable dispersion, individual chains (unimers) and micelles are generally in a dynamic equilibrium; namely, individual chains in the dispersion and inside the micelles are undergoing a constant exchange. As expected, such an exchange for polymer chains is much slower than that for small molecule surfactant. It is rather important to find the time scale related to such an exchange.

From a dynamic point of view, there could exist three types of possible opposite molecular processes at the equilibrium:[12] (1) the self-assembly of unimers to form a new micelle and the disintegration of an existing micelle, (2) the fission of an existing micelle into two small fragments and the fusion of two existing micelles, and (3) the escape and reentry of individual unimers from and into micelles. The assembly or disintegration may become a dominant process in some nonequilibrium cases, such as a sudden change of concentration or temperature or solvent composition. Halperin et al.[13] pointed out that the fission or fusion of large micelles may be kinetically hindered or even fully frozen if the interaction between the insoluble polymer block is sufficiently strong. This leaves the escape and reentry of unimers from and into micelles as the main process in a stable dispersion. The rates of escape and reentry of unimers from and into micelles depend not only on the size of the core but also on the thickness of the shell. To escape, the insoluble block in the core has to move to the boundary between the core and the shell before passing through the shell and diffusing away into the dispersion medium. As expected, the process strongly depends on the copolymer architecture, the chemical nature of the insoluble block, and the interaction between the chain and the selective solvent.

To our knowledge, only a limited number of studied related to the hybridization of polymeric micelles were reported. Munk et al.[12] studied the hybridization of block copolymer micelles by using ultracentrifugation in terms of the sedimentation velocity. They found that the rate of hybridization was very sensitive to the architecture of both copolymers and the thermodynamic properties of the selective solvent. The exchange could be very slow and even frozen when the solvent is very poor for the insoluble block. Recently, Bates et al.[13] further showed that the micellar structures could be completely locked in due to the effect of strong amphiphilicity. Halperin et al.[14] theoretically analyzed the dynamics of unimers in the micelle dispersion and developed some scaling relations for the unimer exchange in several limiting cases. Later, Corti et al.[15] studied the hybridization of polymeric micelles made of different biological amphiphiles in dilute aqueous dispersion mixture and found that the hybridization rate was mainly affected by the cmc. Using the nonradioactive energy transfer (NRET) method, Bendnář et al.[16] found, as expected, that the rate of releasing unimers from a micelle significantly influenced by the compactness (or swelling) of the core and the solvent selectivity. Wang et al.[17] mixed two dispersions of diblock polystyrene-*block*-poly(ethylene oxide) micelles and observed the exchange of unimers only at temperatures higher than 60 °C, presumably due to a stronger interchain interaction at relatively lower temperatures. There are

[†] Chinese Academy of Sciences.
[‡] The Chinese University of Hong Kong.
[§] University of Science and Technology of China.
* The Hong Kong address should be used for correspondence.

10.1021/ma0352936 CCC: $27.50
Published on Web 04/09/2004

Table 1. Characterization of Two Diblock PFS-*b*-PDMS Copolymers and Their Self-Assemble Micelles

sample	M_w[a],PDMS (g/mol)	M_w[a],PFS−*b*−PDM (g/mol)	M_w/M_n	PFS:PDMS[b]	N_{agg}	$\langle R_g\rangle_{micelle}$ (nm)	$\langle R_h\rangle_{micelle}$ (nm)	$\langle\rho\rangle$ (g/cm^3)
PFS_{138}-*b*-$PDMS_{702}$	5.2×10^4	8.6×10^4	1.04	0.2:1	37	18 ± 1	31 ± 1	4.3×10^{-2}
PFS_{235}-*b*-$PDMS_{837}$	6.2×10^4	1.2×10^5	1.07	0.3:1	300	59 ± 2	87 ± 2	2.2×10^{-2}

[a] By GPC. [b] Calculated from the peak areas of ^{1}H NMR at 0.08 and 4.01 ppm.

many open questions, such as the detail of the hybridization pathway and the key factor affected the hybridization rate. To study the hybridization by laser light scattering (LLS), we have to slow down its rate. We decided to introduce ferrocene into the insoluble block to increase the stiffness of the insoluble block and the interaction strength. In this study, polymeric micelles made of diblock copolymers with two different rod−coil block ratios are used to study the hybridization. Our main objective is to have a better understanding of the hybridization pathway.

Experimental Section

Sample Preparation. The samples were prepared under an atmosphere of dry argon with the rigid exclusion of air and moisture using standard Schlenk or cannula techniques or in a glovebox. All chemicals, except otherwise mentioned, were purchased from Aldrich Chemical Co. HPLC grade hexane, pentane, ether, and THF were refluxed several hours and freshly distilled from sodium benzophenone ketyl immediately prior to use. Ferrocene was recrystallized twice from hexane. Me_3SiCl was distilled prior to use. *N*,*N*,*N*′,*N*′-Tetramethylethylenediamine (TMEDA) was stirred over CaH_2 for 10 h and then distilled before use. Hexamethylcyclotrisiloxane ($(Me_2SiO)_3$) was stirred over CaH_2 for 10 h in pentane and then purified by sublimation under vacuum after the removal of solvent. *n*-BuLi (1.6 M in hexane) and silica gel (200−400 mesh) were used as received. ^{1}H NMR spectra were recorded on a Bruker AM-300 spectrometer. All chemical shifts are reported in δ units with reference to internal TMS (0.00 ppm). Molecular weights were estimated by gel permeation chromatography (GPC) using a Waters 515/410/746 instrument equipped with a differential refractometer as the detector. The flow rate was 1.0 mL/min. Polystyrene standards purchased from American Polymer Standards were used for the calibration.

Silicon-bridged [1]ferrocenophane was prepared according to the literature.[18] *n*-BuLi (20 μL, 0.336 M in hexane, 6.72×10^{-3} mmol) was quickly added to a stirred solution of silicon-bridged [1]ferrocenophane (207 mg, 0.855 mmol) in THF (2.5 mL) at room temperature. The color of the solution was changed from red to deep amber during the course of the reaction. 0.5 mL of this solution mixture was taken out and served as PFS homopolymer blocks. A THF solution (2 mL) of $(Me_2SiO)_3$ (60.2 mg, 0.271 mmol) was then quickly added to the above solution of living PFS homopolymers at room temperature. The reaction mixture was stirred for 3 h at room temperature and terminated by the addition of a few drops of Me_3SiCl. The resultant copolymer was precipitated into methanol (ca. 200 mL) in the presence of triethylamine (ca. 2 mL), isolated, and dried under vacuum. The PFS homopolymer was removed by fast column chromatography (SiO_2) using a mixture of cyclohexane/dichloroethane (3:2) as an eluent. The resultant diblock copolymers PFS-6-PDMS were isolated as a yellow solid (2160 mg, 260%). ^{1}H NMR ($CDCl_3$): δ 4.21 (br, Cp*H*), 4.01 (br, Cp*H*), 0.46 (s, $(\eta^5\text{-}C_5H_4)_2FeSi\mathit{Me}_2$), 0.08 (s, $(\mathit{Me}_2SiO)_{3y}$).[18] Characterization of both PFS_{138}-*b*-$PDMS_{702}$ and PFS_{235}-*b*-$PDMS_{837}$ diblock copolymers with a similar PDMS block is summarized in Table 1. The GPC results have been confirmed by static laser light scattering (LLS) measurements. Both the LLS and NMR results are listed in the Supporting Information. The synthetic route is outlined in Scheme 1.

Laser Light Scattering. A commercial LLS spectrometer (ALV/SP-150 equipped with an ALV-5000 multi-τ digital time correlator) and a solid-state laser (ADLAS DPY 425 II, output power is 400 MW at $\lambda = 532$ nm) as the light source were used. The primary beam is vertically polarized with respect to the scattering plane. The details of the LLS instrumentation can be found elsewhere.[19,20] In static LLS, the angular dependence of the excess absolute time-average scattered intensity, known as the Rayleigh ratio $R_{vv}(q)$, of a dilute micelle dispersion with a critical micelle concentration (C_{cmc}) at a total polymer concentration C (g/mL) and scattering angle θ was measured. $R_{vv}(q)$ is related to the weight-average molar mass M_w, the *z*-average root-mean-square radius of gyration $\langle R_g^2\rangle_z^{1/2}$ (or written as $\langle R_g\rangle$), and the second virial coefficient A_2 as[21]

Scheme 1. Synthesis of PFS-*b*-PDMS Diblock Copolymers

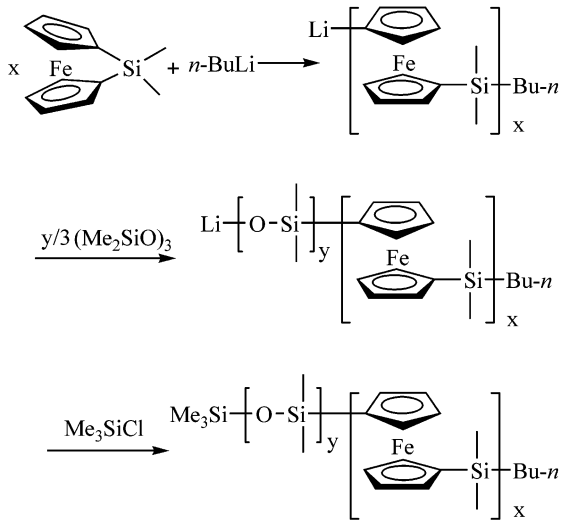

PFS_{138}-*b*-$PDMS_{702}$ x : y = 0.2 : 1

PFS_{235}-*b*-$PDMS_{837}$ x : y = 0.3 : 1

$$\frac{K(C - C_{cmc})}{R_{vv}(q)} \cong \frac{1}{M_w}\left(1 + \frac{1}{3}\langle R_g^2\rangle q^2\right) + 2A_2C \qquad (1)$$

where $K = 4\pi^2n^2(dn/dC)^2/N_A\lambda_0^4$ and $q = (4\pi n/\lambda_0)\sin(\theta/2)$ with N_A, dn/dC, n, λ_0, and θ being the Avogadro number, specific refractive index increment, solvent refractive index, the wavelength of light in vacuo, and the scattering angle, respectively.

In dynamic LLS, the intensity−intensity time correlation function $G^{(2)}(t,q)$ in the self-beating mode can be measured, which is related to the normalized first-order electric field−electric field time correlation function $g^{(1)}(t,q)$ as[22]

$$G^{(2)}(t,q) = \langle I(t,q)\, I(0,q)\rangle = A[1 + \beta|g^{(1)}(t,q)|^2] \qquad (2)$$

where A is a measured baseline, β a parameter depending on the detection optics, and t the delay time. For a polydisperse sample, $|g^{(1)}(t,q)|$ is related to the characteristic line-width distribution $G(\Gamma)$ by[22,23]

$$|g^{(1)}(t,q)| = \frac{\langle E(t,q)\, E^*(0,q)\rangle}{\langle E(0,q)\, E^*(0,q)\rangle} = \int_0^\infty G(\Gamma)\exp(\Gamma)\, d\Gamma \qquad (3)$$

For a pure diffusive relaxation, Γ can be related to the translational diffusion coefficient D by $\Gamma = Dq^2$ at $C \to 0$ and $q \to 0$. $G(\Gamma)$ can be calculated from the Laplace inversion of

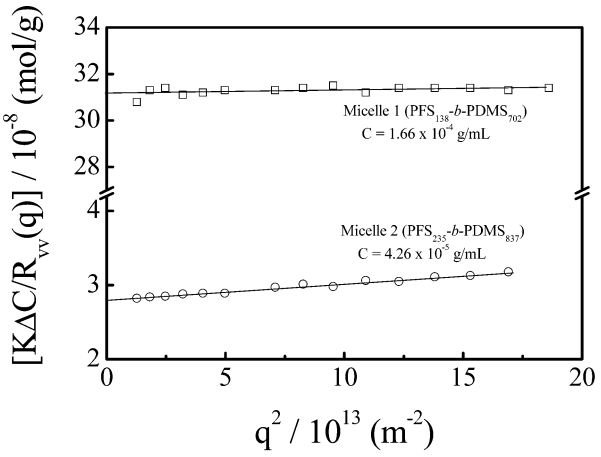

Figure 1. Plot of $K\Delta C/R_{vv}(q)$ vs q^2 for two different kinds of micelles in *n*-hexane at 25 °C, where $\Delta C = C - C_{cmc}$ and the values of C_{cmc} for PFS_{138}-*b*-$PDMS_{702}$ and PFS_{235}-*b*-$PDMS_{837}$ are respectively $\sim 1 \times 10^{-6}$ and $\sim 2 \times 10^{-7}$ g/mL at 25 °C.

the measured $G^{(2)}(t,q)$ on the basis of eqs 2 and 3. The well-accepted Laplace inversion CONTIN algorithm was used. D can be further related to the hydrodynamic radius R_h by $R_h = k_B T/(6\pi\eta D)$, where k_B, T, and η are the Boltzmann constant, the absolute temperature, and solvent viscosity, respectively.

Results and Discussion

n-Hexane is a selective solvent for PDMS but a nonsolvent for PFS.[18,24] In *n*-hexane, diblock copolymers PFS-*b*-PDMS can self-assemble to form polymeric core−shell-like micelles with the insoluble and aggregated PFS blocks as the core and the soluble and swollen PDMS blocks as the shell. Such formed polymeric micelles in dilute dispersion were first characterized by a combination of static and dynamic LLS. The micelles were prepared by first dissolving each block copolymer in THF and then slowly add *n*-hexane into the THF solution to induce the microphase inversion.

Figure 1 shows typical plots of $K\Delta C/R_{vv}(q)$ vs q^2. In a dilute dispersion, the extrapolation of $K\Delta C/R_{vv}(q)$ to $q \rightarrow 0$ leads to an apparent weight-average molar mass of the micelles ($M_{w,micelles}$), and the slope leads to the average radius of gyration $\langle R_g \rangle$. It is helpful to note that C is sufficiently low that the extrapolation of $C \rightarrow 0$ in eq 1 is really not necessary in the present study. The apparent aggregation number N_{agg} can be deduced from $M_{w,micelles}/M_{w,PFS-b-PDMS}$. Table 1 summarizes the values of $\langle R_g \rangle$ and N_{agg}.

On the other hand, Figure 2 shows that, before the mixing, both PFS_{138}-*b*-$PDMS_{702}$ and PFS_{235}-*b*-$PDMS_{837}$ micelles are narrowly distributed. The inset shows that the micelles are very stable over a long time. The values of $\langle R_h \rangle$, defined as $\int_0^\infty f(R_h) R_h \, dR_h$, are also summarized in Table 1. Note that the two diblock copolymers used have a similar PDMS block, but different PFS blocks, which results in polymeric micelles with different sizes. It is reasonable to see PFS_{138}-*b*-$PDMS_{702}$ forms smaller micelles with a smaller aggregation number N_{agg} because its shorter insoluble PFS block provides a weaker aggregation force. It is interesting to note that each PFS_{235}-*b*-$PDMS_{837}$ micelle contains more chains but has a lower apparent chain density $\langle \rho \rangle$ defined as $M_{w,micelle}/(4\pi N_A \langle R_h \rangle^3/3)$. It is known that the PFS block is fairly rigid according to its chemical structure, and the small core is jam-packed with ~300 PFS blocks. Therefore, the lower value of $\langle \rho \rangle$ indicates that the PDMS blocks in the shell must be stretched out due to the steric

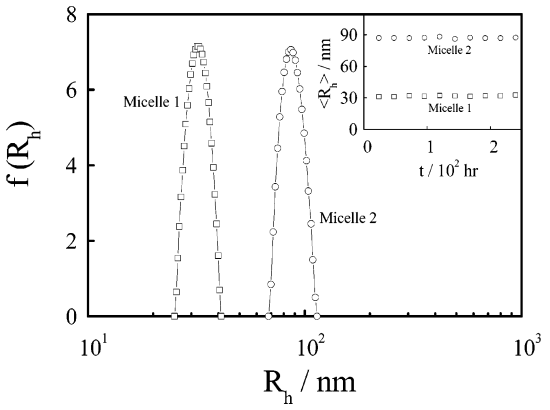

Figure 2. Hydrodynamic radius distributions of two different kinds of micelles at 25 °C. The inset shows the time dependence of average hydrodynamic radius $\langle R_h \rangle$.

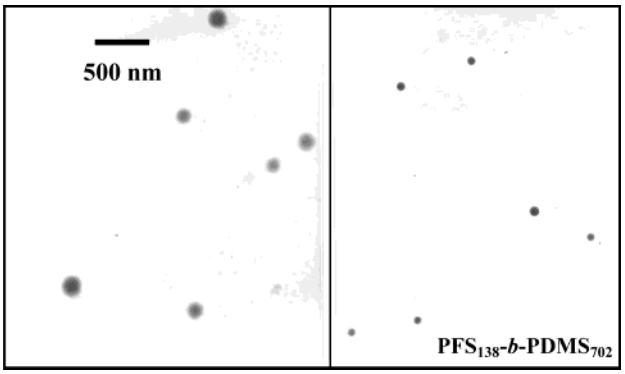

Figure 3. Typical SEM micrographs of PFS_{138}-*b*-$PDMS_{702}$ and PFS_{235}-*b*-$PDMS_{837}$ micelles, where the samples were prepared by a standard SEM method.

repulsion, which increases the thickness and $\langle R_h \rangle$. At the equilibrium, individual chains (unimers) are coexisted with the micelles in the dispersion, but LLS only "sees" large micelles because the scattering intensity is proportional to the square of the mass of a scattering object.

A combination of static and dynamic LLS results shows that the ratio of $\langle R_g \rangle / \langle R_h \rangle$ is even smaller than 0.774 for a uniform hard sphere. This is because the core has a much higher density. Our results are different from those obtained by Winnik et al.[18] They found that PFS-*b*-PDMS block copolymers form wormlike micelles. In comparison with their sample, PFS_{138}-*b*-$PDMS_{702}$ used here has a molar ratio of DMS:FS = 5:1 instead of 6:1, and our PDMS block is about 50% longer than theirs so that our PFS block is much longer. It is known that the morphology is very sensitive to both the block lengths and the molar ratio of the two blocks. The SEM pictures in Figure 3 confirm that the micelles formed in this study are spherical with a size close to those measured in LLS. After separately characterizing the "pure" PFS_{138}-*b*-$PDMS_{702}$ and PFS_{235}-*b*-$PDMS_{837}$ micelles, we mixed the two dispersions together with a volume ratio of $V(PFS_{138}\text{-}b\text{-}PDMS_{702}):V(PFS_{235}\text{-}b\text{-}PDMS_{837}) = 2:1$.

Figure 4 shows that both the time-average scattering intensity $\langle I \rangle_T$ and the overall average hydrodynamic radius $\langle R_h \rangle$ of the solution mixture increase with time. Corti et al.[14] reported a similar result from the mixture of two biological amphiphiles. The Laplace inversion of the measured intensity−intensity time correlation function shows a better view of how the hydrodynamic

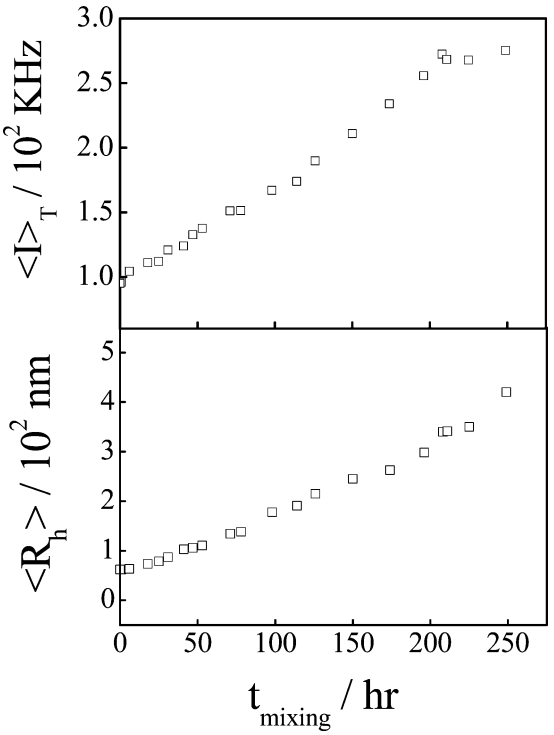

Figure 4. Mixing time dependence of average hydrodynamic radius $\langle R_h \rangle$ and relative time-average scattered light intensity of the solution mixture containing PFS_{138}-*b*-$PDMS_{702}$ ($C = 1.11 \times 10^{-4}$ g/mL) and PFS_{235}-*b*-$PDMS_{837}$ ($C = 1.42 \times 10^{-5}$ g/mL) at 25 °C, where $\theta = 15°$.

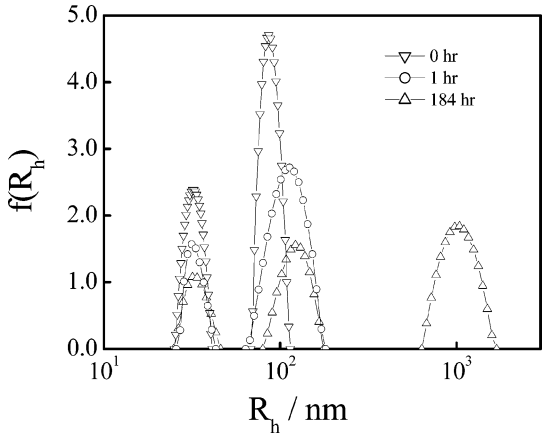

Figure 5. Hydrodynamic radius distributions of different micelles in the solution mixture after different mixing times.

radius changes in terms of its distribution in Figure 5. As expected, just after the mixing, there are only two narrowly distributed peaks located at 31 and 87 nm, corresponding to each kind of "pure" micelle. One hour after the mixing, the position of the peak at 31 nm remains unchanged, but the peak at 87 nm shifts to the direction of larger R_h and becomes broader. As the time elapses, it moves further to the right and finally splits into two peaks. A combination of Figures 4 and 5 indicates the hybridization of micelles in the solution mixture. The increases of both $\langle I \rangle_T$ and $\langle R_h \rangle$ can be attributed to the formation of large hybrid micelles, presumably made of a mixture of PFS_{138}-*b*-$PDMS_{702}$ and PFS_{235}-*b*-$PDMS_{837}$ unimers. The resultant hybrid micelles are also spherical, as shown in the Supporting Information.

Note that before the mixing individual copolymer chains are in a dynamic equilibrium with their corresponding "pure" micelles. After the mixing, the formation of larger hybrid micelles would remove PFS_{138}-*b*-$PDMS_{702}$ and PFS_{235}-*b*-$PDMS_{837}$ unimers from the mixture and destroy the balance, shifting the equilibrium toward individual chains (unimers) so that the number of each kind of the "pure" micelles should decrease. Therefore, the formation of the hybrid micelles should be at the expense of the "pure" micelles. It is known that the Laplace inversion method is extremely sensitive even to a very low level of experimental noise. The inversion result is not reliable if the line-width distribution $G(\Gamma)$ contains more than two relaxation modes. Considering this ill-conditioned problem, we decided to analyze the measured time correlation function by using a nonlinear least-squares fitting of three exponential functions as follows:

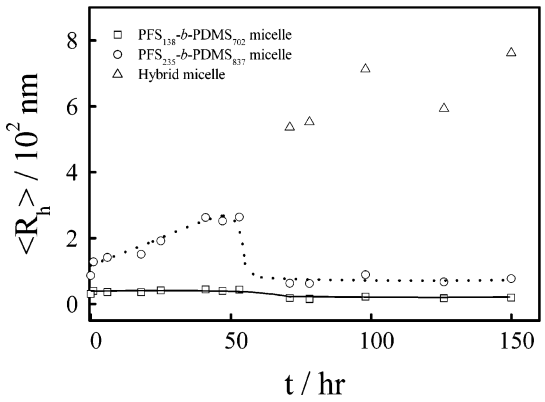

Figure 6. Mixing time dependence of average hydrodynamic radius $\langle R_h \rangle$ of different micelles in the solution mixture.

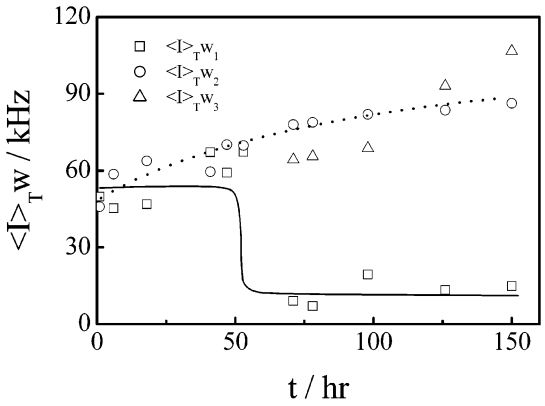

Figure 7. Mixing time dependence of time-average scattered light intensities $\langle I \rangle_T w$ for different micelles in the solution mixture at 25 °C.

$$|g^{(1)}(q,t)| = a_0 + w_1 \exp(-t/\tau_1) + w_2 \exp(-t/\tau_2) + w_3 \exp(-t/\tau_3) \quad (4)$$

where w and τ are the intensity weighting and characteristic decay time of the pure and hybrid micelles, respectively. The subscripts 1, 2, and 3 represent two kinds of the "pure" micelles and the hybrid micelles, respectively. Note that $w_1 + w_2 + w_3 = 1$ and $\tau = 1/\Gamma$. Therefore, each τ can lead to a corresponding average hydrodynamic radius $\langle R_h \rangle$ for each kind of micelle.

A combination of Figures 6 and 7 reveals that when $t < \sim 50$ h, both $\langle R_h \rangle_1$ and $\langle I \rangle_T w_1$ for PFS_{138}-*b*-$PDMS_{702}$ micelles nearly remain a constant. Note that we plot "$\langle I \rangle_T w$ vs t" instead of "w vs t" because $\langle I \rangle_T w$ reflects the intensity of the light scattered from each kind of micelle.

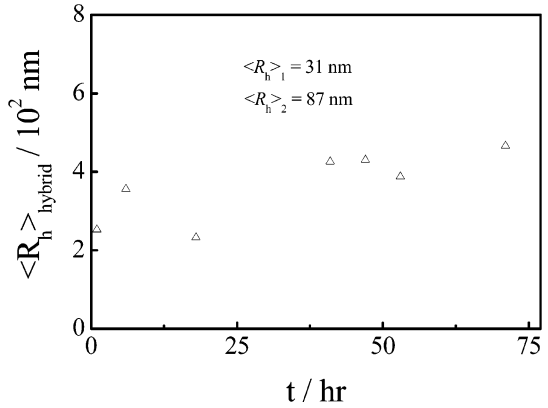

Figure 8. Mixing time dependence of average hydrodynamic radius $\langle R_h \rangle$ of hybrid micelles in the initial mixing stage, where the sizes of PFS_{138}-*b*-$PDMS_{702}$ and PFS_{235}-*b*-$PDMS_{837}$ micelles were fixed in eq 4 during the fitting.

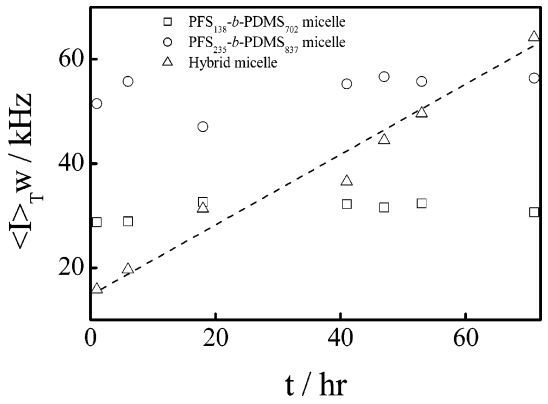

Figure 9. Mixing time dependence of average scattered light intensities $\langle I \rangle_T w$ of three kinds of micelles in the initial mixing stage, where the sizes of PFS_{138}-*b*-$PDMS_{702}$ and PFS_{235}-*b*-$PDMS_{837}$ micelles were fixed in the fitting of eq 4.

During the same time period, $\langle R_h \rangle_2$ related to PFS_{235}-*b*-$PDMS_{837}$ micelles slightly increases, but there is nearly no change in $\langle I \rangle_T w_2$. At ~60 h after the mixing, $\langle R_h \rangle_2$ for PFS_{235}-*b*-$PDMS_{837}$ micelles drops back to ~100 nm, slightly larger than its original value (~81 nm). At the same time, the third peak related to the hybrid micelles appears. Note that at this point $\langle R_h \rangle_1$ decreases to ~28 nm, close to its original value (~31 nm), and $\langle I \rangle_T w_1$ drops significantly from ~50% to ~15%. As the time further elapses, the "pure" micelles coexist with the hybrid micelles in the dispersion, and there is nearly no change in either $\langle R_h \rangle_1$ or $\langle R_h \rangle_2$. It seems that after the mixing the formation of the hybrid micelles is indeed at the expense of PFS_{138}-*b*-$PDMS_{702}$ micelles. In the initial stage (t < 50 h), the number of the hybrid micelles is small, and their size is similar to that of PFS_{235}-*b*-$PDMS_{837}$ micelles. Therefore, it is not possible to resolve them from the peak related to PFS_{235}-*b*-$PDMS_{837}$ micelles. This is why $\langle R_h \rangle_2$ continuously increases in this time period. To have a better understanding of the formation of the hybrid micelles, we can justify the assumption that in the initial period there was no change in the size of either PFS_{138}-*b*-$PDMS_{702}$ or PFS_{235}-*b*-$PDMS_{837}$ micelles. In other words, we can fix τ_1 and τ_2 in eq 4 and try to find how τ_3 as well as w_1 and w_2 change after the mixing.

Figure 8 shows such a fitting result in the first ~70 h after the mixing. $\langle R_h \rangle_{hybrid}$ increases with the time, revealing that the hybrid micelles are formed even in the initial stage just after the mixing, but their size is too close to that of PFS_{235}-*b*-$PDMS_{837}$ micelles. This is why we were not able to separate them when we allowed both τ_1 and τ_2 floating in Figures 5 and 6. On the other hand, Figure 9 shows that in this initial stage most of the scattered light intensity is from the "pure" micelles; namely, they contribute 30% and 55%, respectively. There is no significant change in the intensities of the light scattered from each kind of the "pure" micelles. However, it should be noted that the light intensity from the hybrid micelles increases from ~16 to ~63 kHz. A combination of Figures 8 and 9 reveals that the formation of the hybrid micelles in the initial stage is mainly due to the hybridization of two different kinds of unimers in the mixture, and each kind of "pure" micelle is relatively long-lived. By fixing τ_1 and τ_2 for the entire process, we found that $\langle R_h \rangle_3$ finally reached a plateau of ~700 nm at ~200 h, and at the same time, w_3 increases to ~75%.

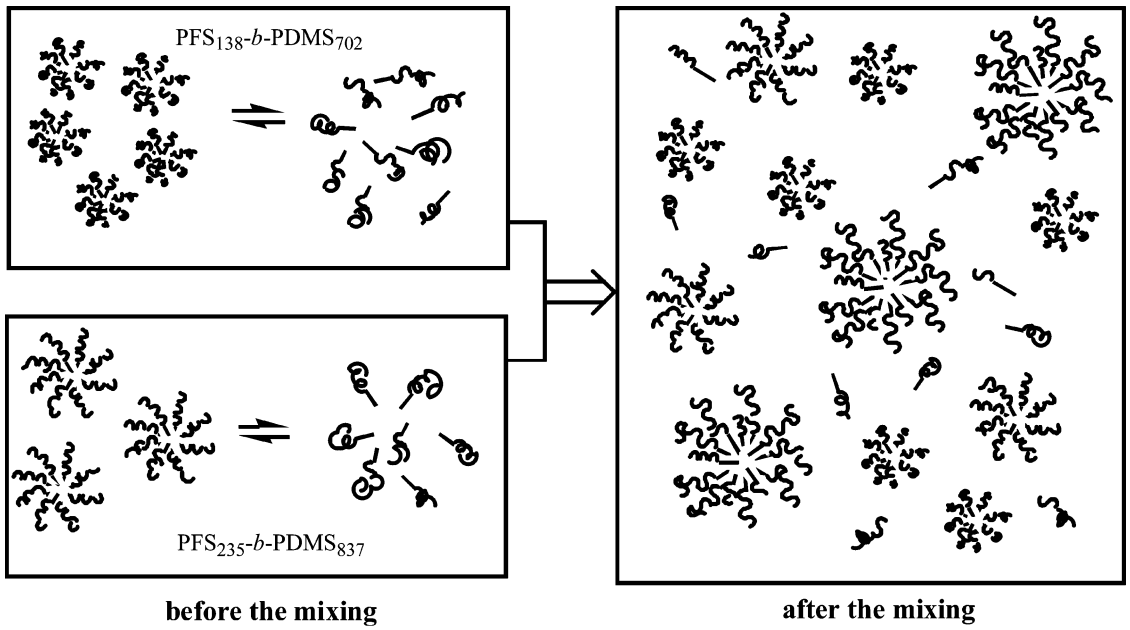

Figure 10. Schematic of hybridization of two different kinds of polymeric micelles.

Figure 10 schematically shows the formation of the hybrid micelles at the expense of PFS_{138}-*b*-$PDMS_{702}$ micelles. In principle, there could exist four different following possible processes: (1) the hybridization of two different kinds of unimers in the mixture, (2) the entry of PFS_{138}-*b*-$PDMS_{702}$ unimers into PFS_{235}-*b*-$PDMS_{837}$ micelles, (3) the entry of PFS_{235}-*b*-$PDMS_{837}$ unimers into PFS_{138}-*b*-$PDMS_{702}$ micelles, and (4) the fusion of two kinds of the "pure" micelles. As mentioned before, Halperin et al.[13] showed that the fission and fusion of polymeric micelles are kinetically hindered or even fully frozen. Note that PFS_{138}-*b*-$PDMS_{702}$ and PFS_{235}-*b*-$PDMS_{837}$ have similar PDMS blocks but different PFS blocks. Also note that PFS_{235}-*b*-$PDMS_{837}$ with a relative longer PFS block has a relatively lower critical micelle concentration (cmc). When the two kinds of "pure" micelles are mixed, the number of PFS_{138}-*b*-$PDMS_{702}$ unimers is much higher than that of PFS_{235}-*b*-$PDMS_{837}$ unimers in the mixture. It is expected that, in comparison with the formation of each kind of the "pure" micelles, the formation of the hybrid micelles gains no extra enthalpy, but the entropy loss should be relatively less because of a gain in the entropy of mixing two different kinds of unimers. In addition, because of the rigidity of the PFS blocks, the hybridization of the PFS blocks with different lengths in the core can reduce the space-filling-induced stress. The facts that $\langle R_h \rangle_2$ becomes slightly larger and $\langle I \rangle_T w_2$ increases after the mixing, as shown in Figures 5 and 6, indicate a possible entry of individual shorter PFS_{138}-*b*-$PDMS_{702}$ unimers into PFS_{235}-*b*-$PDMS_{837}$ micelles. Again, this is driven by the mixing entropy. On the other hand, the constant $\langle R_h \rangle_1$ and the decrease of $\langle I \rangle_T w_1$ reveal that there is nearly no entry of individual longer PFS_{235}-*b*-$PDMS_{837}$ unimers into PFS_{138}-*b*-$PDMS_{702}$ micelles.

Conclusion

Two narrowly distributed PFS-*b*-PDMS diblock copolymers with a similar PDMS block, but different PFS blocks, were synthesized using anionic polymerization. They can self-assemble into polymeric core−shell-like micelles with different sizes in a selective solvent, *n*-hexane. Mixing the two micelle dispersions results in larger hybrid micelles. The study of the hybridization by a combination of static and dynamic laser light scattering (LLS) reveals that larger hybrid micelles are formed from a direct hybridization of two kinds of unimers free in the mixture. The hybridization consumes PFS_{138}-*b*-$PDMS_{702}$ micelles because individual PFS_{138}-*b*-$PDMS_{702}$ unimers are gradually hybrided with PFS_{235}-*b*-$PDMS_{837}$ unimers. It destroys the original dynamic equilibrium between PFS_{138}-*b*-$PDMS_{702}$ unimers and micelles. The hybridization is mainly driven by the mixing entropy and the space filling due to the rigidity of the PFS blocks and at the expense of each kind of "pure" micelle. Our results also indicate that a small amount of PFS_{138}-*b*-$PDMS_{702}$ unimers can enter the PFS_{235}-*b*-$PDMS_{837}$ micelles.

Acknowledgment. This work was supported by the Shanghai-Hong Kong Joint Laboratory in Chemical Synthesis and the Hong Kong Research Grants Council Earmarked Grants (CUHK 403103 and CUHK 4025/02P). Cai o thanks the Croucher Foundation (Hong Kong) for a studentship. We also thank Prof. Changtao Qian and Prof. Yong Tong for helpful discussions.

Supporting Information Available: Zimm plots of PFS_{138} and PFS_{235} in THF. This material is available free of charge via the Internet at http://pubs.acs.org.

References and Notes

(1) Hacziioannou, G.; Patel, S.; Granick, S.; Tirrell, M. *J. Am. Chem. Soc.* **1986**, *108*, 2869.
(2) Milner, S. T. *Science* **1991**, *251*, 905.
(3) Quintana, J. R.; Janez, M. D.; Katime, I. *Polymer* **1998**, *39*, 2111.
(4) Zhu, P. W.; Napper, D. H. *J. Colliod Interface Sci.* **1994**, *164*, 489.
(5) Price, C. In *Developments in Block Copolymers*; Goodman, I., Ed.; Applied Science: New York, 1982; Vol. 1.
(6) Tuzar, Z.; Kaartochvil, P. *Adv. Colloid Interface Sci.* **1976**, *6*, 201.
(7) Leibler, L.; Orland, H.; Wheeler, J. C. *J. Chem. Phys.* **1983**, *79*, 3550.
(8) Noolandi, J.; Hong, K. M. *Macromolecules* **1985**, *15*, 482.
(9) Halperin, A. *Macromolecules* **1987**, *20*, 2943.
(10) Carale, T. R.; Blankschtein, D. *J. Phys. Chem.* **1992**, *96*, 459.
(11) Bunton, C. A.; Yatsimirsky, A. K. *Langmuir* **2000**, *16*, 5921.
(12) Tian, M. M.; Qin, A. W.; Ramireddy, C.; Webber, S. E.; Munk, P.; Tuzar, Z.; Procházka, K. *Langmuir* **1993**, *9*, 1741.
(13) Won, Y. Y.; Davis, H. T.; Bates, F. S. *Macromolecules* **2003**, *36*, 953.
(14) Halperin, A.; Alexander, S. *Macromolecules* **1989**, *22*, 2403.
(15) Cantú, L.; Corti, M.; Salina, P. *J. Phys. Chem.* **1991**, *95*, 5981.
(16) Procházka, K.; Bednář, B.; Mukhtar, E.; Svoboda, P.; Trněná, J.; Almgren, M. *J. Phys. Chem.* **1991**, *95*, 4563.
(17) Wang, Y. M.; Balaji, R.; Quirk, R. P.; Mattice, W. L. *Polym. Bull. (Berlin)* **1992**, *28*, 333.
(18) Massey, J.; Power, K. N.; Manners, I.; Winnik, M. A. *J. Am. Chem. Soc.* **1998**, *120*, 9533. (b) Massey, J.; Temple, K.; Cao, L.; Rharbi, Y.; Raez, J.; Winnik, M. A.; Manners, I. *J. Am. Chem. Soc.* **2000**, *122*, 11577.
(19) Zhang, Y.; Xiang, M.; Jiang, M.; Wu, C. *Macromolecules* **1997**, *30*, 2035.
(20) Wang, X.; Qiu, X.; Wu, C. *Macromolecules* **1998**, *31*, 2972.
(21) Chu, B. *Laser Light Scattering*, 2nd ed.; Academic Press: New York, 1991.
(22) Berne, B. J.; Pecora, R. *Dynamic Light Scattering*; Plenum Press: New York, 1976.
(23) Niu, A. Z.; Li, C. M.; Zhao, Y.; He, J. P.; Yang, Y. L.; Wu, C. *Macromolecules* **2001**, *34*, 460.
(24) Resendes, R.; Massey, J. A.; Dorn, H.; Power, K. N.; Winnik, M. A.; Manners, I. *Angew. Chem., Int. Ed.* **1999**, *38*, 2570.

MA0352936